Angewandte Chemie
Eine Zeitschrift der Gesellschaft Deutscher Chemiker

Supporting Information

Braided Fiber Current Collectors for High-Energy-Density Fiber Lithium-Ion Batteries

X. Huang, C. Wang, C. Li, M. Liao, J. Li, H. Jiang, Y. Long, X. Cheng, K. Zhang, P. Li, B. Wang, H. Peng**

Table of Contents

Experimental Procedures

Materials. The materials used to produce the functional slurries included graphite powder (Shanghai Shanshan, FSN-1), sodium carboxymethyl cellulose (CMC) (Daicel, 2200) and butadiene styrene rubber (SBR) emulsion (JSR, 104A), Super-P (SP) conductive agent (Imerys, Super P Li), LCO (Canrd, MA-EN-CA-0Q), polyvinylidene fluoride (PVDF) binder (Arkema, HSV900), and N-methyl-2-pyrrolidine (Sinopharm, analytical reagent). All of them were used as received without any further purification.

Preparation of braided fiber current collector (BFCC). As shown schematically in **Figure 1c**, the BFCC could be prepared with a braiding machine. First, a commercial ultrathin copper wire was wound around a bobbin, which was then fixed to a spindle. The spindle was fixed to a base disk fastened to the machine bed. By rotating the bobbin, the wire could be fed continuously. The wire was cross braided by the interaction of spindle rotation and restraint by the tightening sleeve. The top take-up device could easily achieve continuous braiding of BFCC for unlimited lengths. The number of axes in the BFCC was determined by the number of feeding spindles.

Preparation of graphite anode. Graphite was selected as the anode active material to estimate the performance of as-fabricated current collectors. Graphite, SP, CMC, and SBR were mixed in the weight ratio of 92:3:1.4:3.6 for slurry preparation, with deionized water as solvent. The solid contents for graphite slurries were 50%. Slurry coating processes were used to coat graphite onto the BFCC. For comparison, graphite slurry was coated on a commercial 200 μm solid Cu current collector. The linear density of the graphite could be tuned by changing the coating speed (**Figure S5a**).

Calculation of the proportion of channels. We assumed that the cross section of a multi-axial braided fiber was approximately circular. Define the percentage of area excluding the metal wire in the cross section as the proportion of channels of the braided fiber. The proportion of channels (ε) of braided fibers could be calculated according to the following equation:

$$\varepsilon = 1 - \frac{n \times \pi \times \left(d/2\right)^2}{\pi \times \left(D/2\right)^2} = 1 - \frac{n \times d^2}{D^2} \quad \text{(Equation 1)}$$

Where n and d were the number and diameter of the braiding wire, respectively, and D was the diameter of braided fiber.

Characterization. Field emission scanning electron microscope (FESEM, Ultra 55) and optical microscopy (Olympus BX51) were used to characterize the surface morphology and the cross section of the current collector and electrode. The diameter of the SFCC and electrode was determined by an electronic micrometer. The diameter of the BFCC was measured with optical microscopy (Olympus BX51). The diameter of each braided fiber was measured every 1 cm along the 10 cm for 10 times. The breaking force was obtained from a universal material tester (Hengyi T0086) with a speed of 2.0 mm·min^{-1}. The resistance (R) was measured by a multimeter to calculate electrical conductivity.

Cell assembly and electrochemical measurements. CR2032 coin cells were assembled in an argon-filled glovebox (O_2, H_2O levels maintained at <0.1 ppm) by the as-prepared anode samples coupled with 0.3 mm thick lithium metal using the electrolyte (Guotaihuarong, LB303) with a sandwiched polypropylene-polyethylene-polypropylene separator (Celgard 2325). Electrochemical performances were measured by a battery testing system (LAND CT2001A). To investigate the capacity, the cells were discharged to 0.005 V and charged to 1 V at 0.1 C. Galvanostatic charge-discharge measurements were carried out at various rates with a cutoff potential window ranging from 0.005 to 1 V. The rate capability of the cells was tested with charging/discharging at increasing current densities (from 0.1 to 1 C). Electrochemical impedance spectra (EIS) over the frequency ranging from 10 kHz to 0.1 Hz with an amplitude of 5 mV was performed on an electrochemical workstation (CHI660E). The cyclic voltammetry (CV) curve was obtained *via* an Autolab (Metrohm) with increasing scanning rates from 0.01 to 1 mV·s^{-1} and increasing potentials from 0.005 to 1 V. FLIBs were assembled with graphite and LCO as anodic and cathodic active materials, respectively. The LCO cathodes consisted of 92 wt% of LCO, 3 wt% of SP, and 5 wt% of PVDF with Al wire (diameter 200 μm) as current collectors. The linear capacity ratio for the negative electrode to the positive electrode was approximately 1.1. Charge-discharge measurements were performed using a LAND-CT2001A battery test system. The FLIBs were galvanostatically charged at 0.3 C from 3 to 4.4 V and then charged at 4.4 V until the current was below 0.05 C rate. The FLIB was discharged to 3 V at 0.5 C. To test the rate performance, FLIBs were discharged at increased current densities (*i.e.*, 0.1, 0.3, 0.5, 0.7, and 1 C) and charged at a constant 0.2 C in a voltage window of 3-4.4 V. The internal resistances of FLIBs were analyzed by a CHI 660C electrochemical workstation with a frequency range from 100 kHz to 0.001 Hz.

Finite element simulations. The battery's symmetry along its height allowed for a two-dimensional cross-sectional model to be developed, as illustrated in **Figure S16**. The model showed the position of the Cu current collector, graphite electrode, separator, lithium metal, and other specific positions. The dimensions of each component were marked in the figure. The thickness of the metal was neglected because of the electrochemical reaction occurring only on the surface of the lithium metal and the high electron conductivity. The Batteries and Fuel Cells Materials Library in the software were used to set up the material properties for the electrolyte and electrode materials. The electrolyte was $LiPF_6$ in 1:1 EC: DMC with an initial concentration of 1 M. The positive electrode was the graphite electrode which consisted of a mixture of 40% electrode and 40% electrolyte with an initial lithium concentration of 10 mol·L^{-1}. The exchange total current density was set as –0.01 A. For this reaction, the equilibrium potential and equilibrium potential temperature derivative were both set as 0 V. 150 min time-dependent solver was set up to store the solution at 5 min intervals.

Fabrication of textile battery. The textile battery was prepared by weaving the FLIBs. The size of the textile battery was tunable for different application scenarios. The textile battery prepared by weaving eight 0.2-m-long FLIBs was used for stability evaluation. The textile battery with forty 1-m-long FLIBs was used to charge the cell phone. For differentiation, LCO||BFCC-G FLIBs were woven into the pink fabric, while LCO||SFCC-G FLIBs were woven into the purple fabric.

Results and Discussion

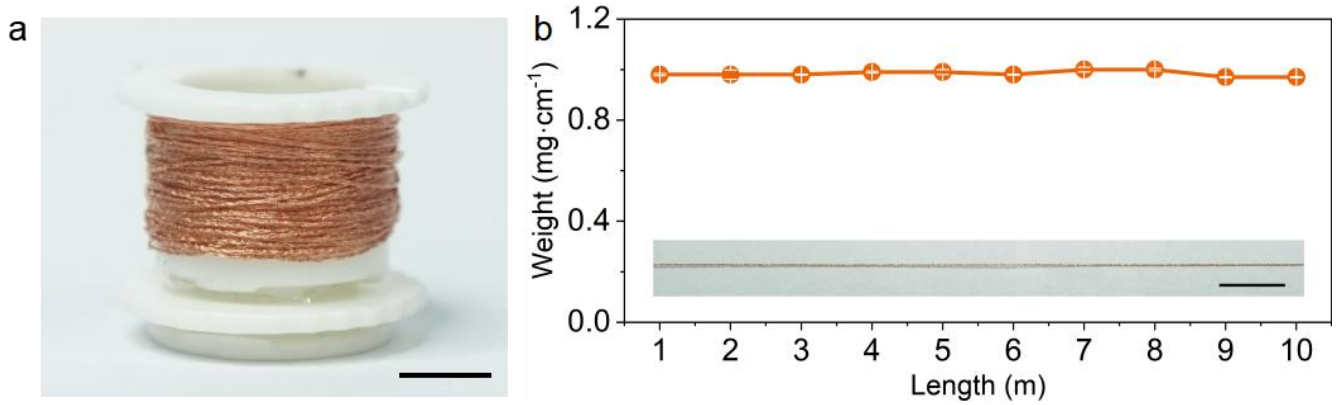

Figure S1. (**a**) Photograph of a bobbin wrapped with a 10 m multi-axial braided fiber. Scale bar, 1 cm. (**b**) Weight per centimeter of the six-axis braided fiber of 50 μm Cu wire being maintained with increasing lengths (inset, photograph of the braided fiber). Scale bar, 1 cm.

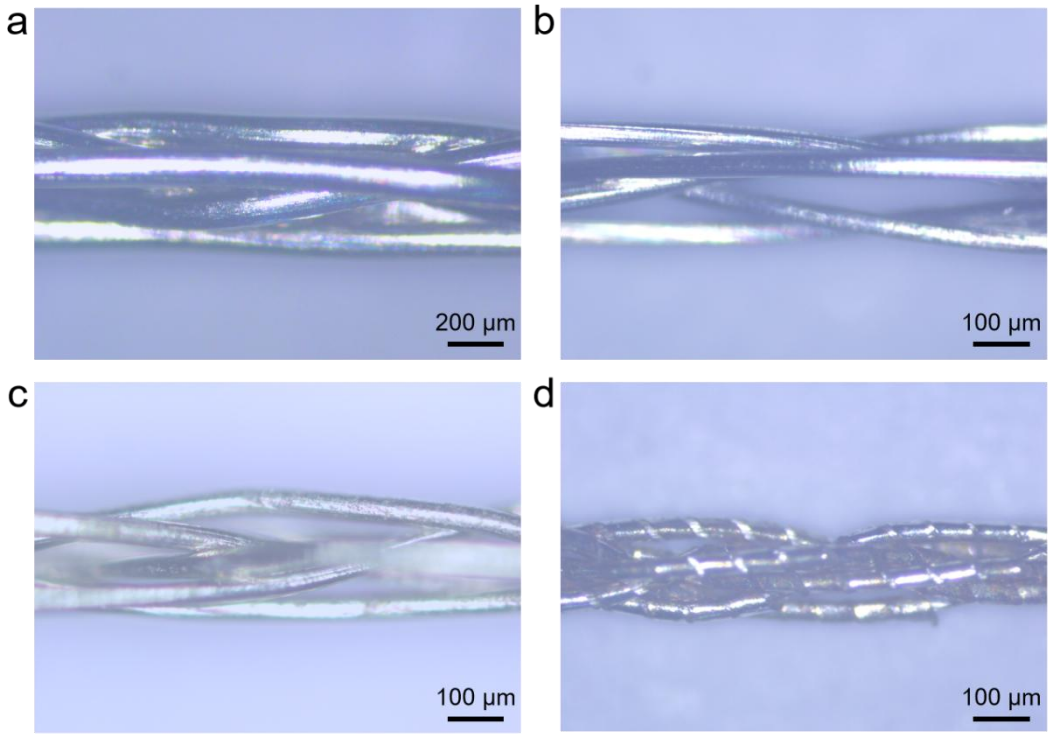

Figure S2. Optical micrographs of braided fiber current collectors consisting of (**a**) aluminum wire, (**b**) stainless steel wire, (**c**) nickel wire, and (**d**) nylon wire.

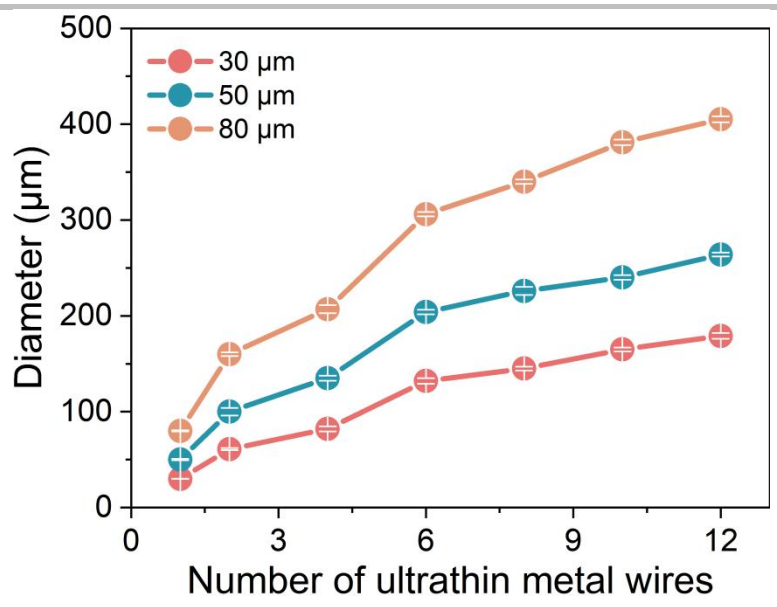

Figure S3. Effect of the braiding parameters on the diameter of braided fibers.

The diameter increased with the increasing number of braiding ultrathin metal wires, and the trend of increase became progressively slower. The cross sections of multi-axial braided fibers were assumed to be approximately circular.

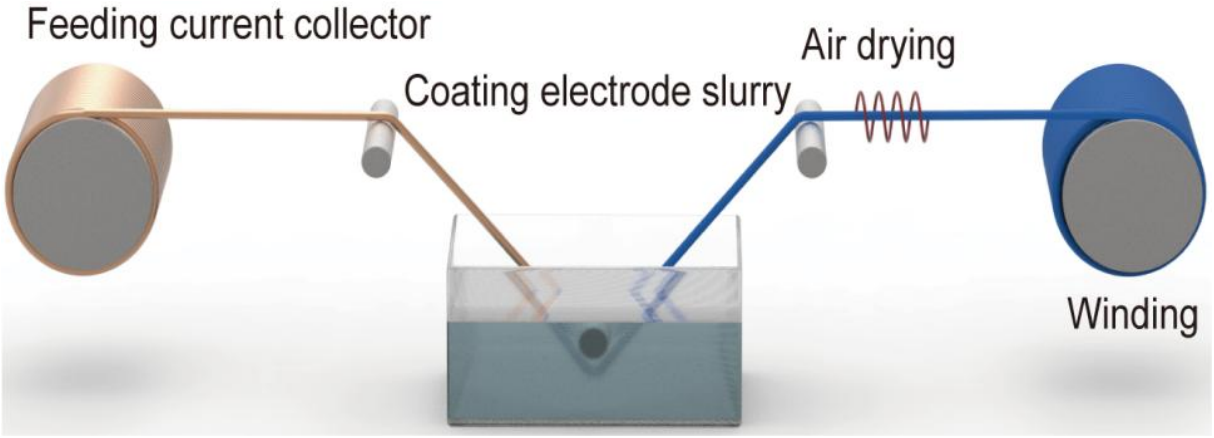

Figure S4. Schematic of the set-up used to produce continuous graphite electrode. The graphite slurry was coated on SFCC and BFCC to obtain SFCC-G and BFCC-G electrodes, respectively.

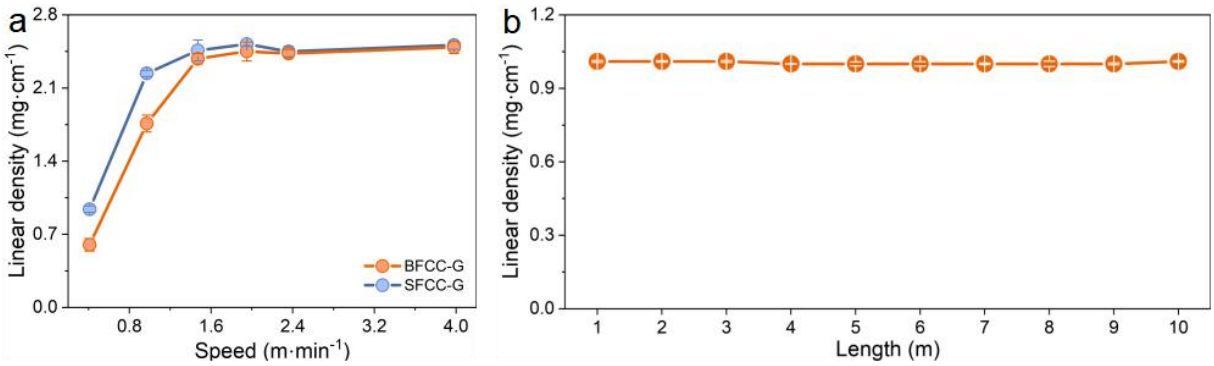

Figure S5. (**a**) Linear density of graphite increased with increasing coating speed. (**b**) Linear density of graphite being maintained with increasing lengths (BFCC-G).

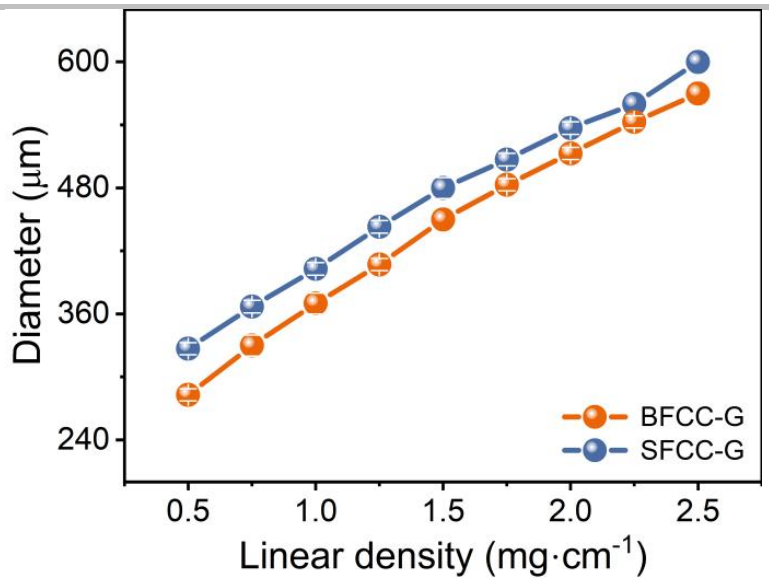

Figure S6. Relationship between diameter of fiber electrode and linear density of loaded graphite.

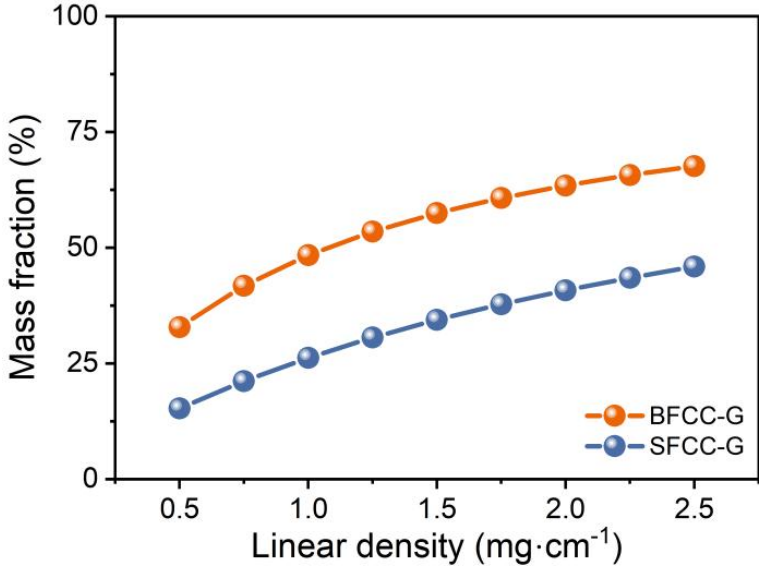

Figure S7. Relationship between mass fraction of graphite and its linear density on the fiber electrode.

Here, graphite accounted for 92% of the total mass of the active layer. The linear density of the BFCC and SFCC were 0.98 and 2.73 mg·cm^{-1}, respectively. The mass fraction of graphite on the electrode could be calculated as:

$$\text{Mass fraction} = \frac{m_{\text{graphite}}}{m_{\text{current collector}} + {}^{m_{\text{graphite}}}/_{0.92}} \quad \text{(Equation 2)}$$

Where m_{graphite} was the linear density of graphite on the fiber electrode, and $m_{\text{current collector}}$ was the linear density of fiber current collector.

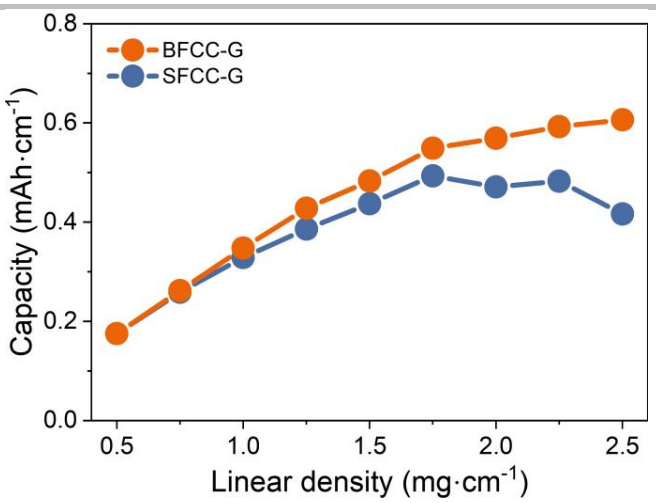

Figure S8. Trends of graphite electrode capacity with the increasing linear density of loaded graphite.

In the range of 0.5-2.5 mg·cm^{-1}, the capacity of the BFCC-G electrode kept increasing with the increasing active materials. However, the capacity of the SFCC-G electrode showed a tendency to increase first, then stabilize, and finally decrease slightly.

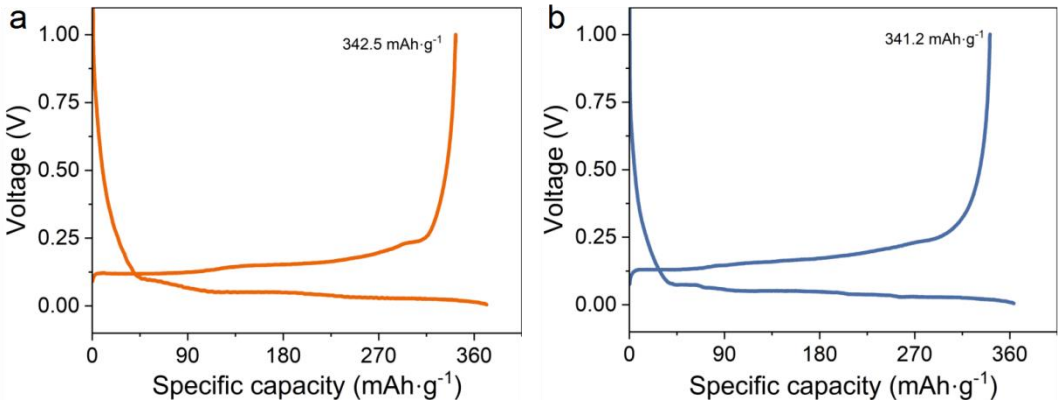

Figure S9. Charge/discharge voltage *versus* specific capacity curves of (**a**) BFCC-G electrode with 1.25 mg·cm^{-1} graphite and (**b**) SFCC-G electrode with 0.9 mg·cm^{-1} graphite.

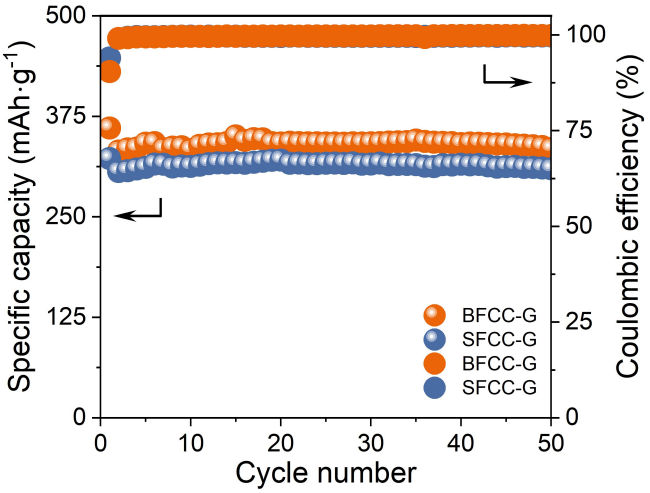

Figure S10. Cycling performance of BFCC-G and SFCC-G electrodes at 0.1 C. The first cycle was set as 0.05 C to form a stable solid electrolyte interface.

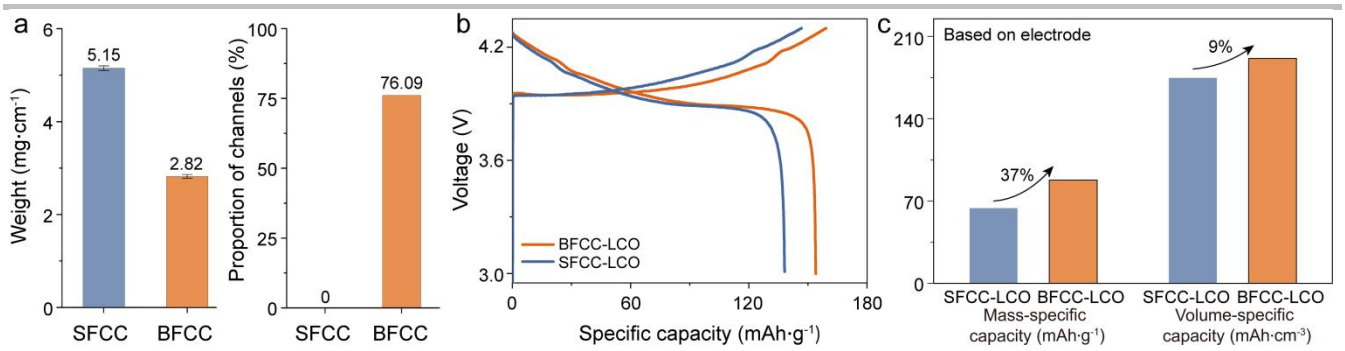

Figure S11. (**a**) Weight and proportion of channels of braided fiber Al current collector and solid fiber Al current collector. (**b**) Charge/discharge curves of LCO electrodes with high loading content of linear density of 5 mg·cm^{-1} fabricated by two types of Al current collectors. (**c**) Comparison in mass/volume specific capacities based on the whole electrode.

The braided fiber Al current collector with a diameter of ~500 μm was composed of six 100 μm Al wires as braids. While the solid fiber Al current collector with a comparable diameter of 500 μm was selected as the control sample.

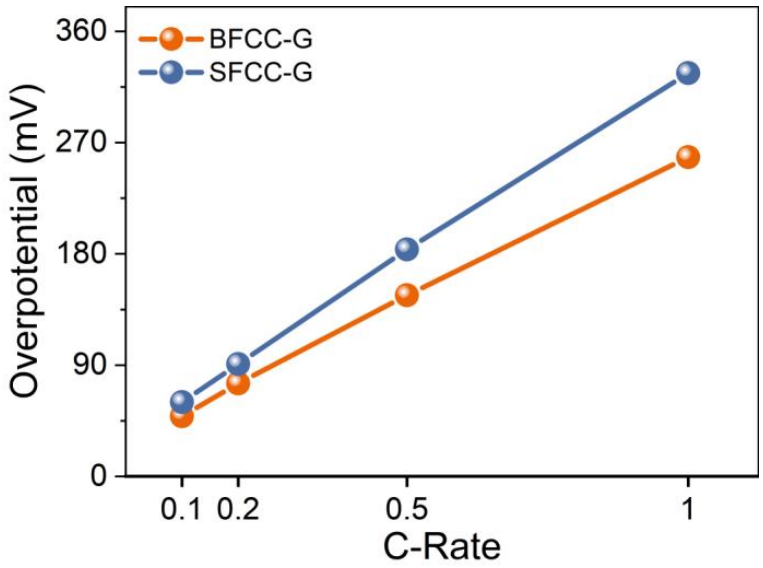

Figure S12. Relationship between overpotential and rate of BFCC-G and SFCC-G electrodes with 1.25 mg·cm^{-1} graphite.

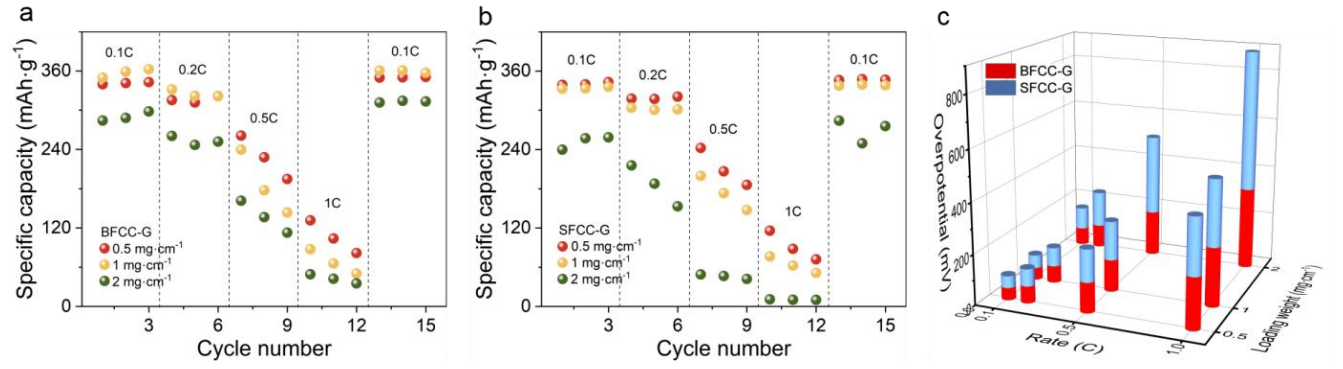

Figure S13. (**a**, **b**) Rate performance of BFCC-G and SFCC-G electrodes with increasing linear densities of graphite, respectively. (**c**) Overpotential of BFCC-G and SFCC-G electrodes with increasing linear densities of graphite at different rates.

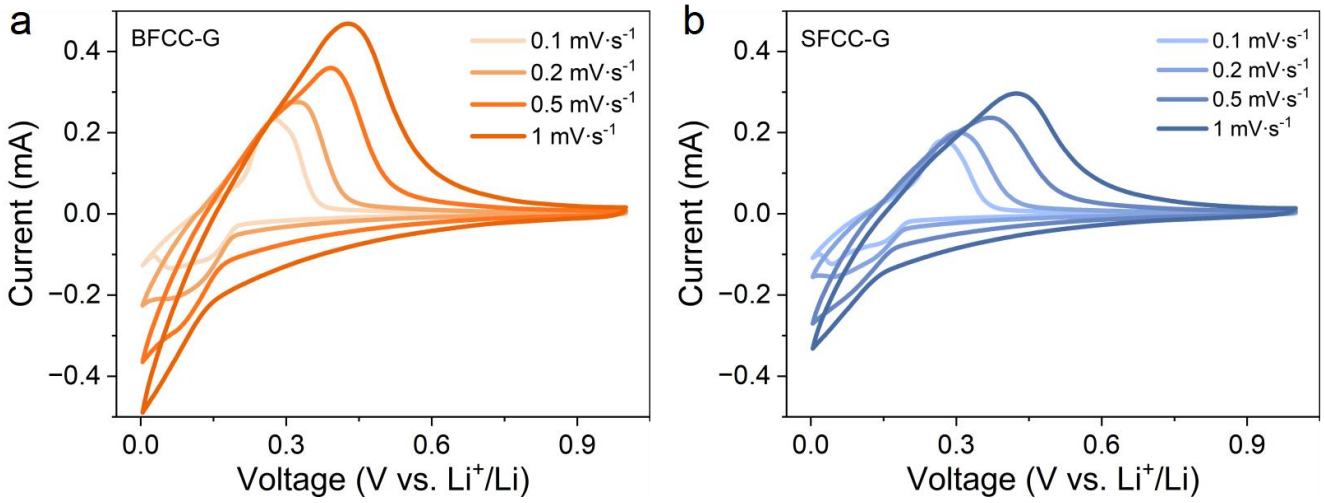

Figure S14. CV curves of (**a**) BFCC-G and (**b**) SFCC-G electrodes at increasing scan rates from 0.1 to 1 mV·s^{-1}.

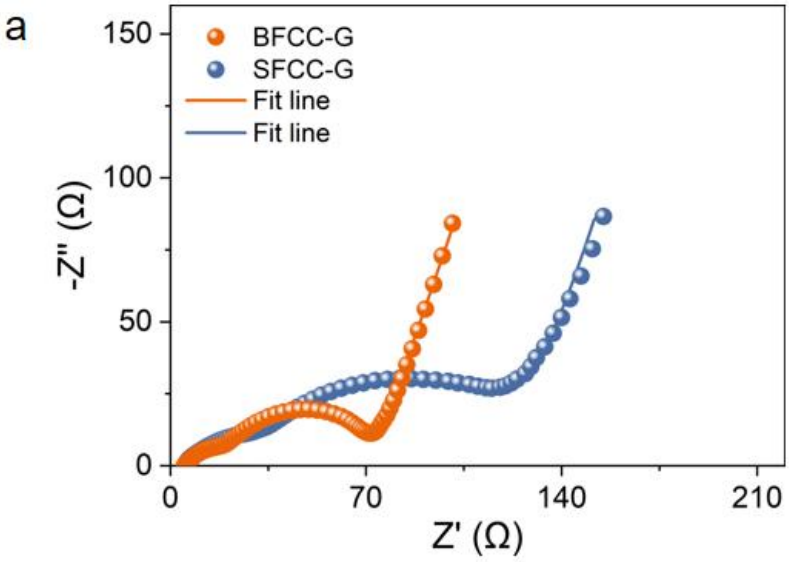

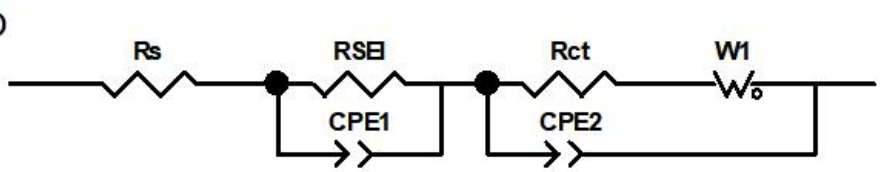

c

	BFCC-G	SFCC-G
R_{ct} (Ω)	49.3	74.4

Figure S15. (**a**) Nyquist plots of BFCC-G and SFCC-G electrodes after 1 cycle at 0.1 C. (**b**) Equivalent circuit model consisting of R_s (ohmic resistance of the electrolyte), R_{SEI} (interfacial layer resistance), R_{ct} (charge transfer resistance), CPE (corresponding constant phase element about the double layer capacitance), and W (Warburg impedance). (**c**) Corresponding fitting results of R_{ct}.

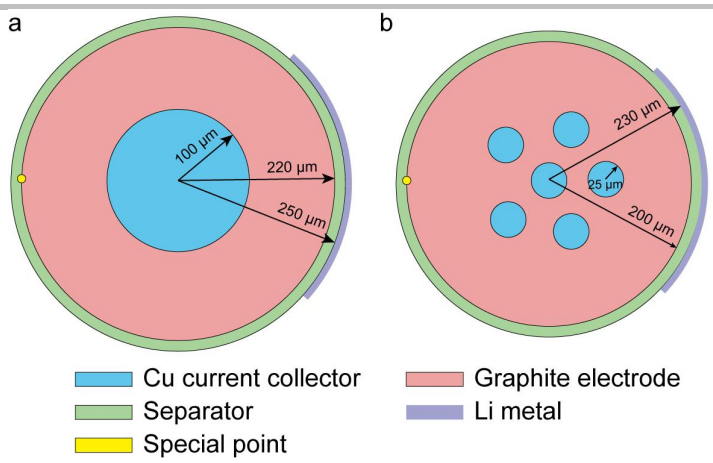

Figure S16. Cross-sectional layout of half-cells of (a) SFCC-G and (b) BFCC-G consisting of Cu current collector, graphite electrode, separator, and lithium foil anode. The yellow points were selected as the special points to record simulated Li-ion concentrations over time.

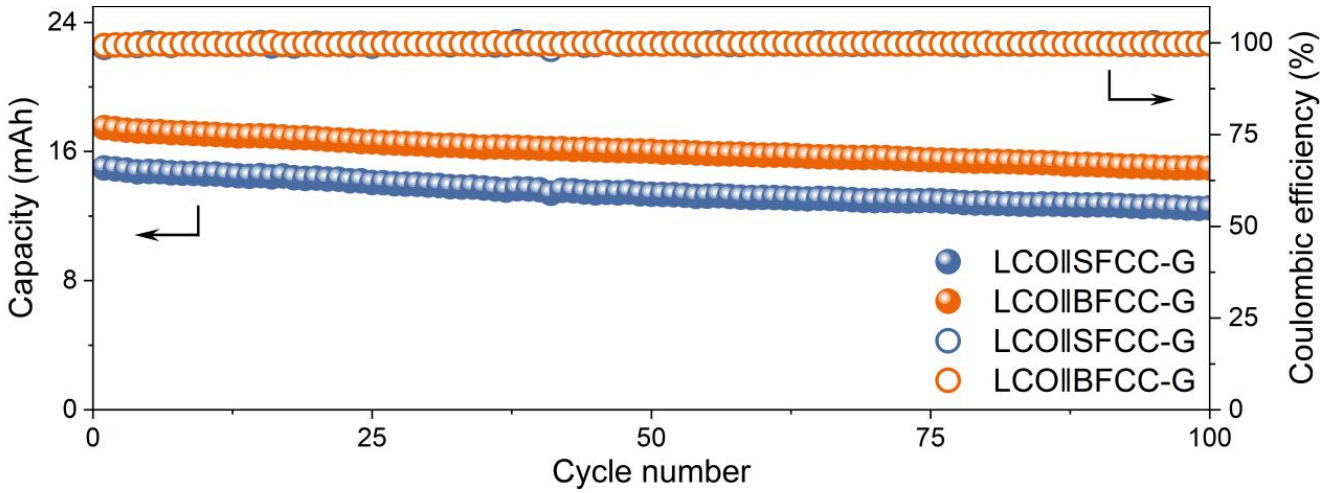

Figure S17. Cycling performance of FLIBs with 0.5 m length for SFCC-G and BFCC-G electrodes.

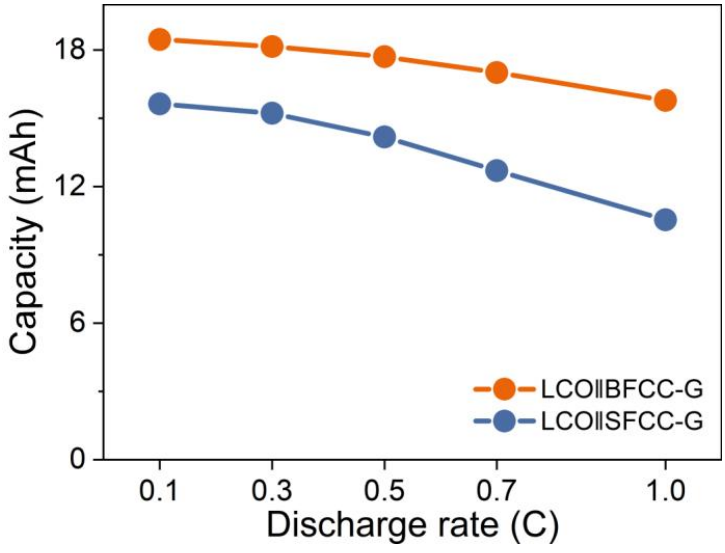

Figure S18. Capacity of LCO||BFCC-G and LCO||SFCC-G FLIBs with 0.5 m length at increasing discharge rates.

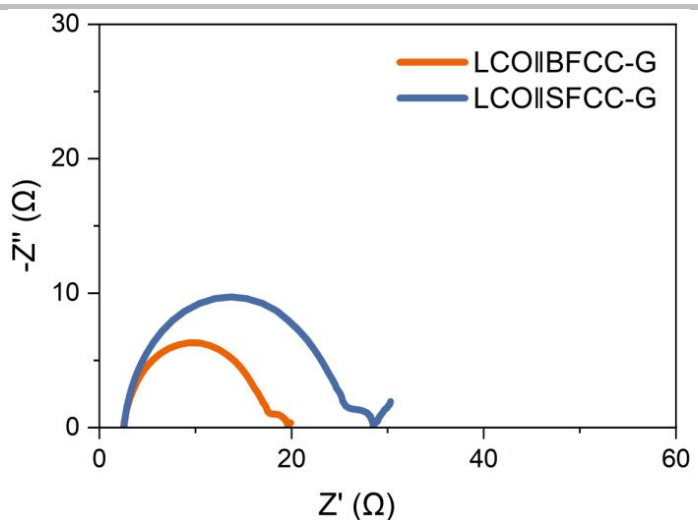

Figure S19. Nyquist plots of the LCO||BFCC-G and LCO||SFCC-G FLIBs with 0.5 m length. The FLIBs showed the same charged state of 50%.

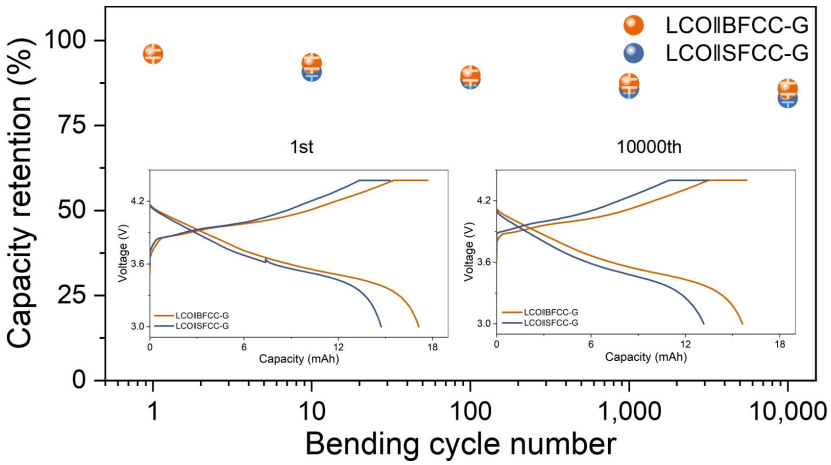

Figure S20. Capacity retention under cyclic bending of LCO||BFCC-G and LCO||SFCC-G FLIBs. Inset: charge-discharge curves at the 1st and 10, 000th bending cycle number.

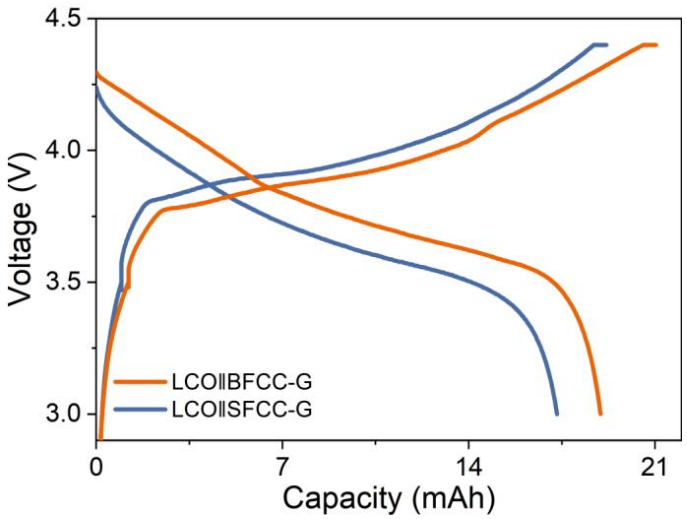

Figure S21. Charge and discharge curves of LCO||BFCC-G and LCO||SFCC-G FLIBs used to calculate energy density.

Figure S22. An FLIB textile consisting of eight 0.2-m-long LCO‖BFCC-G FLIBs to power light-emitting devices. The FLIB textile size was about 0.2 m×0.1 m.

Figure S23. The soaked textile battery as shown in **Figure 4h** powering light-emitting diodes after wringing out the water.

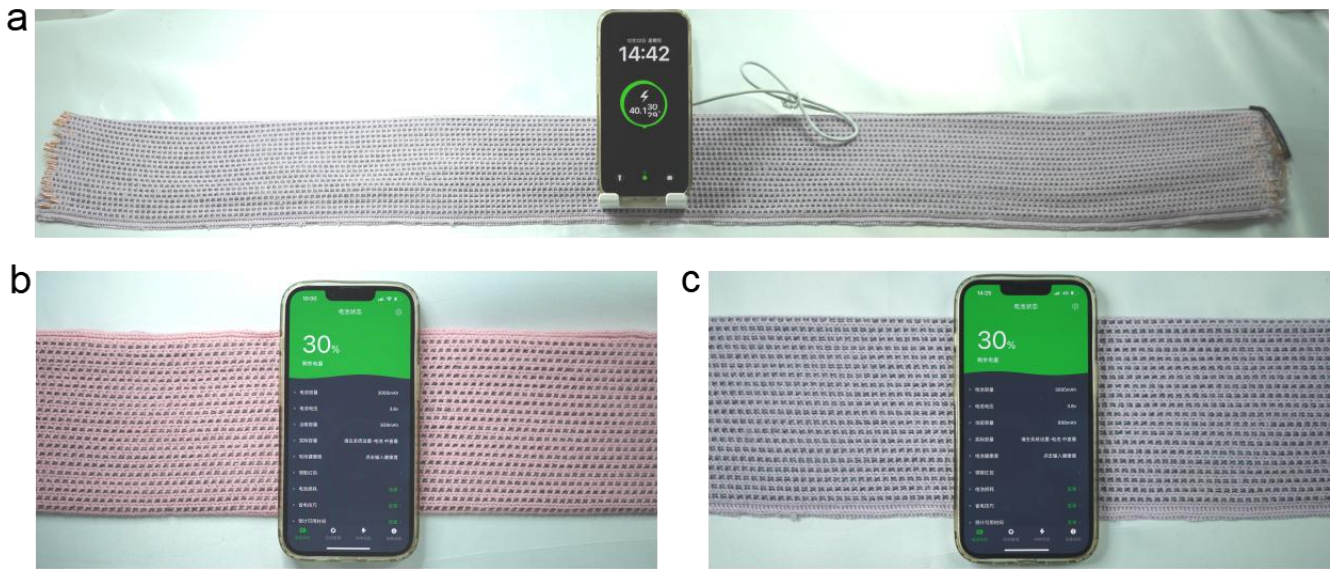

Figure S24. (**a**) An FLIB textile woven from forty 1-m-long LCO‖SFCC-G FLIBs to charge a cell phone. The FLIB textile with size of appropriately 1 m×0.3 m was folded and only twenty FLIBs were shown in the photograph. (**b**, **c**) The power of the cell phone before charging with LCO‖BFCC-G and LCO‖SFCC-G FLIB textiles, respectively.

Table S1. Calculated specific energies of LCO||SFCC-G and LCO||BFCC-G FLIBs, and their corresponding cell parameters.

Item	LCO||SFCC-G	LCO||BFCC-G
Cathode (mg)	113.9	125.2
Anode (mg)	58.4	59.8
Al current collector (mg)	70.5	71.3
Cu current collector (mg)	117.8	43.2
Separator (mg)	17.6	17.4
Electrolyte (mg)	448	447
Polymer composite tube (mg)	382	380
Tab (mg)	18.7	18.7
Total Weight (mg)	1226.9	1162.6
Discharge capacity (mAh)	17.314	18.952
Discharge energy (mWh)	63.909	71.696
Specific energy ($Wh \cdot kg^{-1}$)	52.09	61.67

Author Contributions

H. Peng and B. Wang conceived and directed the research project. X. Huang and C. Wang designed the experiments, analyzed the data, and wrote the manuscript. H. Jiang, Y. Long, K. Zhang and P. Li helped with characterizations. C. Li, M. Liao, X. Cheng, and J. Li provided helpful advice on the working mechanism analysis. All authors discussed the results and commented on the manuscript.